NANO LETTERS

Letter

pubs.acs.org/NanoLett

Room Temperature Semiconductor–Metal Transition of $MoTe_2$ Thin Films Engineered by Strain

Seunghyun Song,[†] Dong Hoon Keum,[†,‡] Suyeon Cho,[†] David Perello,[†] Yunseok Kim,*[,§] and Young Hee Lee*[,†,‡]

[†]Center for Integrated Nanostructure Physics, Institute for Basic Science (IBS), [‡]Department of Energy Science, Department of Physics, and [§]School of Advanced Materials Science and Engineering, Sungkyunkwan University, Suwon 440-746, Korea

Supporting Information

ABSTRACT: We demonstrate a room temperature semiconductor–metal transition in thin film $MoTe_2$ engineered by strain. Reduction of the 2H-1T′ phase transition temperature of $MoTe_2$ to room temperature was realized by introducing a tensile strain of 0.2%. The observed first-order SM transition improved conductance ~10 000 times and was made possible by an unusually large temperature-stress coefficient, which results from a large volume change and small latent heat. The demonstrated strain-modulation of the phase transition temperature is expected to be compatible with other TMDs enabling the 2D electronics utilizing polymorphism of TMDs along with the established materials.

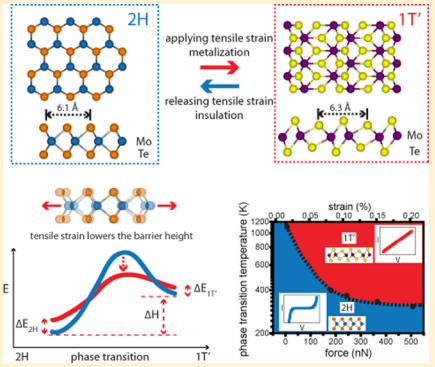

KEYWORDS: *Strain, phase transition, semiconductor-metal transition, modulation, $MoTe_2$*

Polymorphism of 2D transition metal dichalcogenides (TMDs), an intriguing feature by its own, holds immense potential in the development of 2D electronics. For instance, the homojunction formed between the metallic and the semiconducting phases of TMDs has been shown to be Ohmic,[1] offering a viable solution to the contact issue on the 2D electronics.[2] Moreover, the polymorphism expands the diversity to already existing library of 2D materials, providing additional building blocks.[1,3−7] However, despite the recent developments, technology utilizing phase transitions and the accompanying semiconductor–metal transition remains largely unexplored. A particular hurdle in working with phase transitions in TMDs is the high temperature requirements. There have been only a limited number of methods to obtain phase transition, i.e., either through heating[8,9] (laser or e-beam irradiation) or chemical modifications,[1,6] which usually involves a lattice distortion of the treated materials. On the other hand, strain has been a useful tool to modulate the transition temperature of different materials such as ferromagnetic–paramagnetic,[10,11] metal–insulator,[12] superconducting,[13,14] and others.[15] In addition, the 2D nature of the TMDs implies facile application of in-plane tensile strain to the thin film making strain a very attractive modulator for phase engineering.

To explore strain modulated phase transition in TMDs, we chose molybdenum ditelluride ($MoTe_2$) as a model system for its unique properties. It has two stable phases: semiconducting 2H (hexagonal; ~1 eV bandgap) and metallic 1T′ (distorted octahedral) phases. Furthermore, the phase transition temperature of $MoTe_2$ is known to be extremely sensitive to tellurium deficiency/excess ranging from 650 to 900 °C.[8,16] The high sensitivity of the transition temperature to tellurium deficiency/excess suggests that the transition temperature of $MoTe_2$ should exhibit similarly high sensitivity to other stimuli such as strain.

In this Letter, we used mechanical strain to control the phase transition temperature of $MoTe_2$ and demonstrate reversible phase transition at room temperature under ambient conditions. A first-order phase transition from 2H to 1T′ was induced under a small tensile strain of 0.2%, which was applied using an atomic force microscope (AFM) tip while phase was identified by current AFM (CAFM). It was found that increased levels of strain resulted in a reduction of the phase transition temperature from ~900 °C to room temperature. Furthermore, the observed SM phase transition at room temperature was fully reversible under ambient conditions after release of strain.

Figure 1a shows ball-and-stick atomic structures of the 2H and 1T′ phases of $MoTe_2$. When observed from the top view, the positions of Te atoms in the 2H phase overlap with each other to maintain hexagonal symmetry. For the 1T′ phase, the Te atoms are offset as the coordination is distorted, and the in-plane lattice constant between Te atoms is extended by ~3% (6.3 Å vs 6.1 Å), as shown in Figure 1a. The 2H phase is semiconducting with a bandgap of 1 eV, whereas the 1T′ phase

Received: August 29, 2015
Revised: December 19, 2015
Published: December 29, 2015

DOI: 10.1021/acs.nanolett.5b03481
Nano Lett. 2016, 16, 188−193

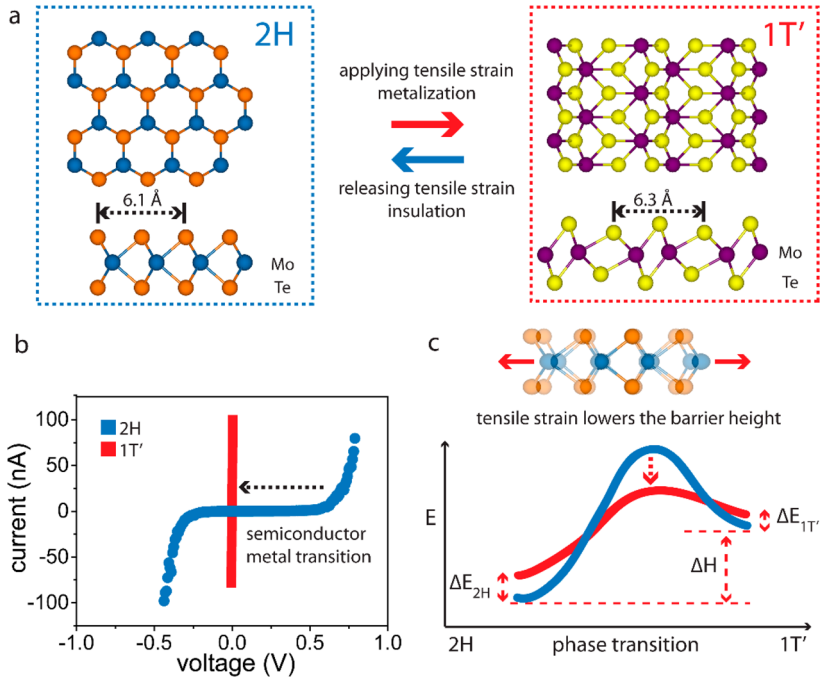

Figure 1. Controlling phase transition of $MoTe_2$ and accompanying semiconductor−metal transition by strain. (a) Atomic structures of 2H and 1T′ $MoTe_2$. Polymorph of $MoTe_2$ is controlled by in-plane tensile strain. (b) Semiconductor−metal transition. Semiconductor−metal transition accompanies the 2H to 1T′ phase transition as observed by the change in the IV curves. (c) Schematic view of phase transition barrier modulated by strain. Under tensile strain, the activation energy of the phase transition is lowered, resulting in a lowered phase transition temperature.

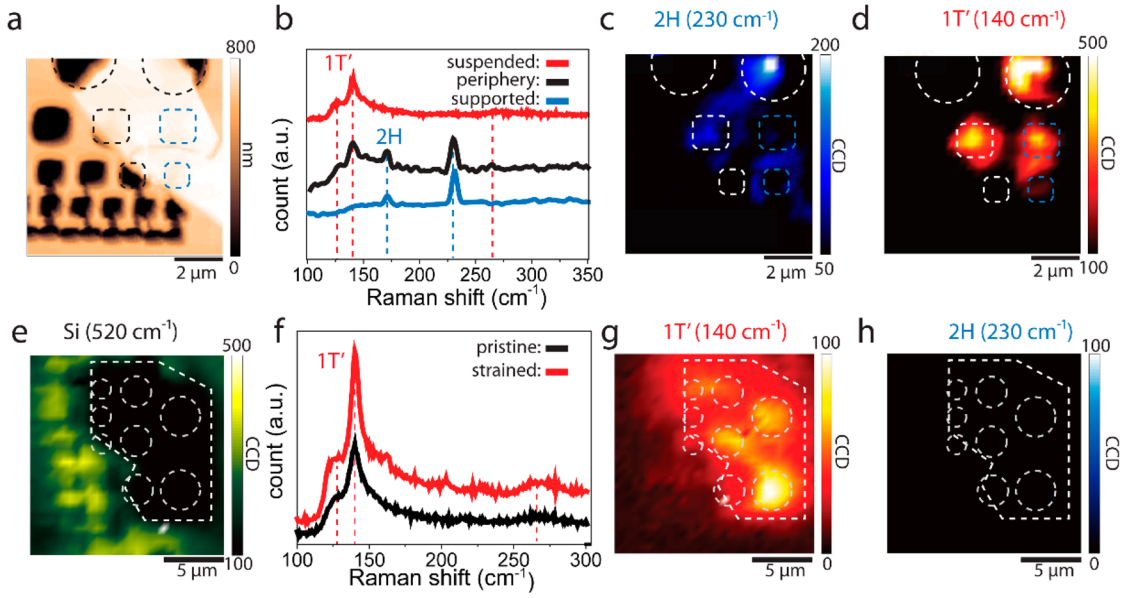

Figure 2. AFM/Raman study of suspended $MoTe_2$. (a) AFM topography image of the suspended 2H $MoTe_2$ flake (thickness of ∼20 nm) obtained from noncontact mode. Circles (squares) outline the cavities partially (fully) covered by $MoTe_2$. (b) Raman spectra taken at the outside (supported), periphery, and the center (suspended) of the cavities showing different Raman signatures of 2H and 1T′ under 0.2% strain. Initially, the entire film started with the 2H phase. (c) Raman intensity mapping near 230 cm^{-1} (2H) with a spectral width of 20 cm^{-1}. 2H Raman signal is absent in the two fully covered cavities outlined in squares, indicating phase transition from 2H to 1T′. (d) Raman intensity mapping near 140 cm^{-1} (1T′) with a spectral width of 20 cm^{-1}. 1T′ Raman signal emerged within the cavities, with higher intensity in the larger cavities due to the increased strain. (e) The position of 1T′ $MoTe_2$ is identified by the intensity mapping near 520 cm^{-1} (Si). The Si peak intensity is also weakened by the presence of the 1T′ $MoTe_2$ thin film. The sample (the underlying cavities) is (are) outlined by white-dashed lines (in circles). (f) Raman spectra taken at the suspended region of 1T′ $MoTe_2$ before and after straining, featuring no phase change. (g) Raman intensity mapping images near 140 cm^{-1} (1T′) with a spectral width of 20 cm^{-1}. The entire film is in the 1T′ phase. The intensity is stronger at the suspended regions due to enhanced out-of-plane mode due to the absence of substrate. (h) Raman intensity mapping near 230 cm^{-1} (2H) with a spectral width of 20 cm^{-1}. No indication of the 2H phase is observed.

DOI: 10.1021/acs.nanolett.5b03481
Nano Lett. 2016, 16, 188−193

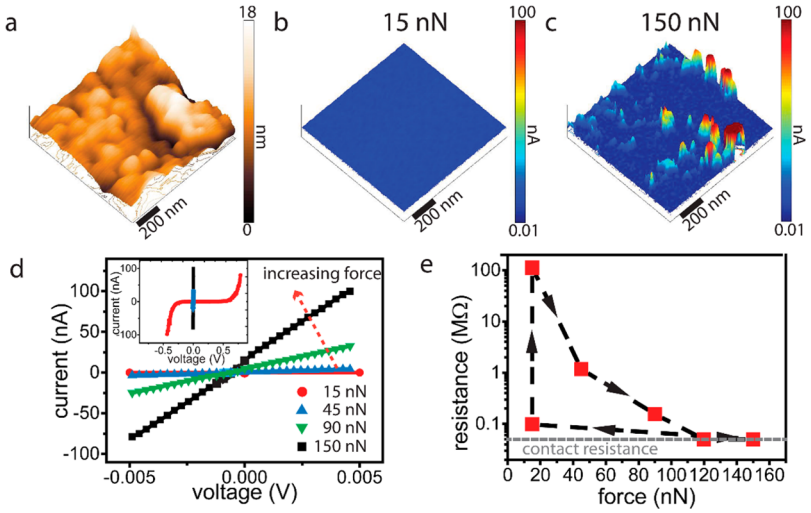

Figure 3. Current mapping with various forces in CAFM. (a) AFM topography image of 2H $MoTe_2$ film on Au/Si substrate. Rough gold surface with a maximum height difference of ~18 nm is shown with local hills and valleys. (b–c) Current mappings of the same region with 5 mV bias under different contact forces of 15 and 150 nN. Color map is in a log scale. Clear topology dependence of the current peaks was observed by comparing *a* with *c*. (d) *I*/*V* curves taken at different forces are plotted, clearly showing the metallization of 2H $MoTe_2$ film under tensile strain. The current level increased about 4 orders of magnitude. IV curve changed from double Schottky junction to an Ohmic curve (inset). (e) The resistance of system is plotted with the arrows denoting the sequence of scans. The reversible metallization of 2H $MoTe_2$ is shown.

is semimetallic[8,17] and displays increased low-bias conductivity (Figure 1b). The tensile-strain-modulated phase transition of 2H-$MoTe_2$, shown schematically in Figure 1c, can be understood in terms of a reduction of the activation energy barrier in the transition state and modulation of cohesive energy of each phase in response to strain.

To demonstrate the occurrence of a 2H-1T′ phase transition under uniform tensile strain, the sample was prepared as follows. First, cavities with different diameters were patterned on a Si substrate (Figure S1a), followed by the transfer of a $MoTe_2$ thin film using poly(methyl methacrylate)/poly(vinyl alcohol)/SiO_2 floating-film method (see details in Supporting Information). AFM topography image of the suspended 2H-$MoTe_2$ (~20 nm) film is shown in Figure 2a. Raman intensity mapping and contact-mode AFM scans were simultaneously performed (as depicted in Figure S1b) with a contact force of 200 nN which corresponds to 0.2% of strain (Figure S2). The in-plane elastic modulus of the material was calculated as 140 GPa, which is in good agreement with a theoretical prediction and similar to elastic modulus of MoS_2.[17,18]

From the Raman spectra taken at the supported and suspended regions presented in Figure 2b, evidence of phase transition from 2H to 1T′ is observed only in the suspended regions. These areas show representative 1T′ Raman peaks (120, 140, and 270 cm^{-1}),[8] while the supported region show only 2H $MoTe_2$ peaks (170 and 230 cm^{-1}).[19] Raman intensity near 230 cm^{-1} (2H phase) is also weaker inside the cavities, most notably in the fully covered cavities outlined by blue dashed circles. Conversely, an Raman intensity near 140 cm^{-1} (1T′ phase) emerges within the cavities, featuring a signature of 1T′ $MoTe_2$ (Figure 2d). The transition is not uniform in the partially suspended regions (outlined by white dashed circles) as both 2H and 1T′ phases coexist. This is ascribed to anisotropic stress applied to the $MoTe_2$ film during AFM scanning.

A similar experiment was carried out on a native 1T′ $MoTe_2$ film. The outline of the $MoTe_2$ film was identified by the Raman signal of the silicon substrate (520 cm^{-1}) as it was screened by a 20 nm thick 1T′ film (Figure 2e). No phase transition was observed under tensile strain as presented in the pristine and strained Raman spectra of the suspended 1T′ $MoTe_2$ (Figure 2f). No appreciable change was observed between the two spectra, indicating that the crystal structure remained unchanged under tensile strain. The Raman intensity mappings at 140 (1T′) and 230 (2H) cm^{-1} shown in Figure 2g–h demonstrate that the film remained as 1T′ without any indication of emerging 2H. The higher Raman intensity at the cavities can be attributed to enhanced out-of-plane modes and different reflection interface (air as opposed to Si) in the suspended regions. This stable 1T′ phase under tensile strain can be understood by the extended lattice constant, as shown in Figure 1a. Moreover, the phase transition from 2H to 1T′ by in-plane tensile strain observed here is congruent with theoretical predictions.[17,20−23]

To further examine the changes in electrical properties accompanying strain-induced 2H (semiconductor)-1T′ (metallic) phase transition, CAFM measurements were carried out under different contact forces. For this, a Au film was deposited on SiO_2/Si substrate and was used as a counter electrode for the CAFM measurements. Subsequently, 5 nm thick 2H $MoTe_2$ thin film was transferred onto the Au film. The CAFM tip was used to apply force to the $MoTe_2$ film,[24,25] and I–V curves were measured simultaneously. The AFM topography image (Figure 3a) of the investigated regions shows clear hills and valleys, resulting from inherent surface roughness (R_{rms} of 2.42 nm) of the deposited Au film on SiO_2 /Si substrate (See also Figure S3). These valleys (with length and width on the order of 100 nm) created locally suspended $MoTe_2$ regions, allowing tensile strain to be applied through the AFM tip (diameter of 25 nm). Figures 3b-c shows the current mapping at a bias voltage of 5 mV in response to different contact forces. For 15 nN applied force, no appreciable current change is observed, independent to the positions of hills and valleys (Figure 3b). As the force increases, the current level starts to rise, in particular near the valleys, by 4 orders of magnitude at 150 nN (Figure 3c). The topological dependence of the current

DOI: 10.1021/acs.nanolett.5b03481
Nano Lett. 2016, 16, 188–193

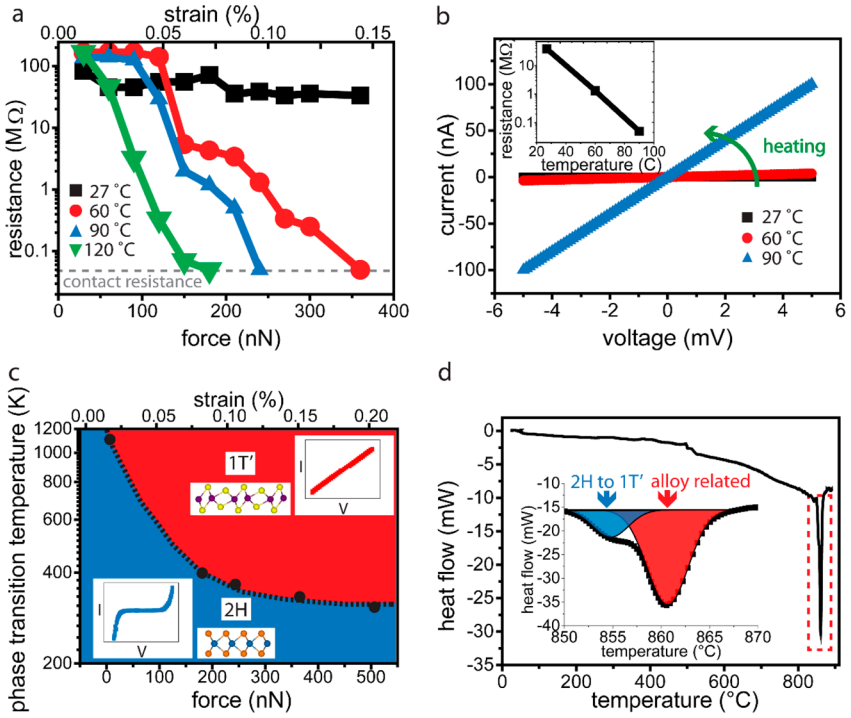

Figure 4. Modulating the phase transition temperature of $MoTe_2$ by strain. (a) Force vs resistance plots at different temperatures. The graph shows that the resistance of the system converging to the contact resistance with smaller forces at elevated temperatures. (b) *IV* curves taken under 250 nN at different temperatures. The phase transition occurred around 90 °C under a strain, confirming the phase transition temperature modulation by strain. The inset shows the resistance as a function of temperature changing nearly 4 orders of magnitude. (c) Temperature-force phase diagram for semiconducting 2H and metallic 1T′ $MoTe_2$. (d) DSC results on 2H $MoTe_2$ powder. Two endothermic peaks were observed at 855 and 860 °C corresponding to 2H-1T′ phase transition and the alloy-related transition due to Te loss.

peaks is also observed from a scattered plot of height and current as the high current level is exclusively observed in the valleys (Figure S4). The I–V curves taken at different contact forces indicates a SM transition as the I–V changes from a double Schottky junction to Ohmic (inset of Figure 3d). Detailed descriptions of the electrical system formed between the tip and the substrate are provided in Figure S5.

After confirming the phase transition at 150 nN, the force was reduced back to the initial level under 15 nN (Figure 3e). Interestingly, a portion of the film (~50 nA) remained metallic during the first 15 nN scan immediately following the 150 nN scan. The retained metallicity is attributed to some portions of the film that had not been reverted back to 2H phase within the scan time (~40 min). In the second 15 nN scan, the current recovered to the original semiconducting state. The resistance of the system as a function of force under 5 mV bias is summarized in Figure 3e, where metallization under tensile strain and resulting phase reversal after release of strain is shown. The large resistance change of nearly 4 orders of magnitude under increased contact force cannot be explained exclusively by the improved contact of AFM tip but by the associated phase transition from semiconducting to metallic $MoTe_2$. This process was fully cyclic without an appreciable baseline resistance change. A detailed study on the reversal dynamics is provided in the Supporting Information (Figure S6), where the initial 2H phase is shown to be completely recoverable within several tens of minutes after strain release.

To explore engineering of phase transition temperature by strain, a set of CAFM experiments at different temperatures was also performed on a 5 nm 2H $MoTe_2$ film prepared on Au/SiO_2/Si substrate (the flake of 5 nm $MoTe_2$ is shown in Figure S7a). The sample was heated to different temperatures, and the required force to induce SM transition was monitored by CAFM at each temperature. Figure 4a shows the resistance as a function of applied force (and the corresponding strain) at different temperatures. At room temperature, no phase transition occurs up to 360 nN. The increase in the force required (compared to the sample in Figure 3) to induce a phase transition is due to a reduced surface roughness (R_{rms} 0.24 nm) and an absence of local valleys to facilitate the application of local tensile strain. Under the same force, however, the phase transition is triggered at 60 °C. At elevated temperatures, the required force (strain) to activate the phase transition is reduced further, indicating clear dependence of the phase transition temperature by strain. Note that temperatures above 120 °C were unavailable due to the indium contacts used to connect the gold surface to the AFM system. Figure 4b shows *I*–*V* curves at various temperatures for a fixed force of 250 nN, demonstrating a phase transition at 90 °C under contact force of 250 nN. The resistance of the system decreases by nearly four orders as shown in the inset of Figure 4b (also see Figure S7b–d), confirming a SM transition.

Figure 4c summarizes the temperature-force phase diagram showing the phase boundary as a function of both applied force and temperature. The corresponding in-plane strain can be *estimated* to be *the same order of magnitude* (in the order of 0.1%) as the AFM/Raman study using a simple vertical compression model (because of the uncertainty in the exact strain distribution, only the order of magnitude of the quantified strain values should be considered). The modulation of the phase transition temperature is given by the Clausius–Clapeyron equation[12,15,26] as $dT/d\sigma = \Delta VT/\Delta H$, where T is

DOI: 10.1021/acs.nanolett.5b03481
Nano Lett. 2016, 16, 188–193

the transition temperature, σ is the stress, ΔV is the volume change during phase transition, and ΔH is the latent heat of the phase transition. Typically, the modulation of the phase transition temperature follows a linear trend in response to stress; however, in this work, the phase transition temperature deviates from a linear trend as ΔT becomes comparable to the transition temperature itself:

$$T = T_0 \exp\left(\frac{\Delta V}{\Delta H}\sigma\right) + T_1 \quad (1)$$

The slope of the modulation, $dT/d\sigma$, was 0.16 K/MPa at room temperature, which is about 10 times larger than the reported value of VO_2.[12] The volume expansion during the phase transition is estimated to be about 1.4% per unit $MoTe_2$. This value was obtained by comparing the unit cells of 2H and 1T′ phases (Figure S8). By fitting the experimental data to eq 1 using the estimated volume change, we obtained $\Delta H \sim 330$ cal/mol. This value is much smaller than 950−1200 cal/mol in the SM transition of VO_2,[12,26] implying the SM transition in $MoTe_2$ to be energetically more favorable.

To rationalize our observations, we performed differential scanning calorimetry (DSC) on $MoTe_2$ powder to measure the latent heat. A large endothermic peak is observed at ∼860 °C (see red dotted box in Figure 4d), indicating that the 2H-1T′ phase transition is first order. The zoomed-in version, shown in the inset of Figure 4d, reveals that the peak can be decomposed into two Gaussian peaks with center temperatures of 855 and 860 °C. To elucidate the origin of these endothermic peaks, thermal gravimetric analysis (TGA) was further performed (Figure S9a). TGA reveals a gradual mass loss starting from 500 °C, with total mass loss reaching 40% by 950 °C. The rate of the mass loss is relatively constant up to 800 °C, and it increases sharply revealing a phase transition near 890 °C. The increased rate of post phase transition mass loss (shown by the red dotted lines in Figure S9a) suggests that the resulting phase (1T′) is more susceptible to Te vaporization compared to the initial phase (2H). This susceptibility of 1T′ phase to Te vaporization results in a large mass loss immediately following the phase transition (Figure S9b). Thus, we rationalize that the two distinct endothermic peaks correspond to two different origins. The first endothermic peak (centered at 855 °C in the inset of Figure 4d) corresponds to the 2H-1T′ phase transition, albeit with Te deficiency. The second endothermic peak (centered at 860 °C in the inset of Figure 4d) is triggered by the severe Te loss following the 2H-1T′ phase transition and is considered to be phase change driven by the modified stoichiometry. From the first endothermic peak, the latent heat of the 2H-1T′ phase transition was estimated to be 360 cal/mol. This value is congruent with the extracted value from the stress-temperature diagram, 330 cal/mol, validating the diagram shown in Figure 4c, although the direct comparison may not be accurate due to different Te-deficiency.

In summary, tensile strain was used to control the phase transition temperature of semiconducting 2H to metallic 1T′ $MoTe_2$ and to induce phase transition at room temperature. It was found that, under small tensile strains, the phase transition temperature was tunable down to room temperature. Further, a homogeneous and reversible phase transition was shown at room temperature at a tensile strain of 0.2%. The demonstrated strain-engineered phase transition could be applied to other TMDs and with different stimuli other than heating (such as electric field, chemical doping and more). The enormous change in electrical properties accompanying phase transition suggests developments of extremely sensitive sensors where a small amount of strain will lower the transition temperature so that a small change in the environment could trigger phase transition. This concept can be applied in developing sensors for optical, biological and electrical applications. Moreover, this could expand the fabrication of tailored 2D electronics using not only different materials but also the different phases of the utilized materials.

■ ASSOCIATED CONTENT

Supporting Information

The Supporting Information is available free of charge on the ACS Publications website at DOI: 10.1021/acs.nanolett.5b03481.

Experimental descriptions, sample preparation methods, sample description and characterization, reversal dynamics of 1T′-2H phase transition following the strain release, estimation of volume change accompanying 2H-1T′ phase transition, and the thermal gravimetric analysis results (PDF)

■ AUTHOR INFORMATION

Corresponding Authors

*E-mail: yunseokkim@skku.edu.
*E-mail: leeyoung@skku.edu.

Notes

The authors declare no competing financial interest.

■ ACKNOWLEDGMENTS

We thank Sera Kim for assisting aligned transfer; Heejun Yang for discussion; Daehee Seol for assisting AFM operation; Sungtae Kim for assisting operation of NT-MDT; Hyun Ah Moon for operating DSC. This work was supported by IBS-R011-D1.

■ REFERENCES

(1) Kappera, R.; et al. *APL Mater.* **2014**, *2*, 092516.
(2) Geim, A. K.; Grigorieva, I. V. *Nature* **2013**, *499*, 419−425.
(3) Voiry, D.; et al. *Nat. Chem.* **2014**, *7*, 45−49.
(4) Wang, Y. C.; et al. *ACS Nano* **2013**, *7*, 10083−10093.
(5) Wang, Q. H.; Kalantar-Zadeh, K.; Kis, A.; Coleman, J. N.; Strano, M. S. *Nat. Nanotechnol.* **2012**, *7*, 699−712.
(6) Kappera, R.; et al. *Nat. Mater.* **2014**, *13*, 1128−1134.
(7) Guo, H.; Lu, N.; Wang, L.; Wu, X.; Zeng, X. C. *J. Phys. Chem. C* **2014**, *118*, 7242−7249.
(8) Keum, D. H.; et al. *Nat. Phys.* **2015**, *11*, 482−486.
(9) Lin, Y. C.; Dumcenco, D. O.; Huang, Y. S.; Suenaga, K. *Nat. Nanotechnol.* **2014**, *9*, 391−396.
(10) Pertsev, N. A.; Zembilgotov, A. G.; Tagantsev, A. K. *Phys. Rev. Lett.* **1998**, *80*, 1988−1991.
(11) Haeni, J. H.; et al. *Nature* **2004**, *430*, 758−761.
(12) Cao, J.; et al. *Nat. Nanotechnol.* **2009**, *4*, 732−737.
(13) Takahashi, H.; Igawa, K.; Arii, K.; Kamihara, Y.; Hirano, M.; Hosono, H. *Nature* **2008**, *453*, 376−378.
(14) Gao, L.; et al. *Phys. Rev. B: Condens. Matter Mater. Phys.* **1994**, *50*, 4260−4263.
(15) Wang, Y.; Ren, X.; Otsuka, K.; Saxena, A. *Acta Mater.* **2008**, *56*, 2885−2896.
(16) Clarke, R.; Marseglia, E.; Hughes, H. P. *Philos. Mag. B* **1978**, *38*, 121−126.
(17) Hughes, H. P.; Friend, R. H. *J. Phys. C: Solid State Phys.* **1978**, *11*, L103.
(18) Bertolazzi, S.; Brivio, J.; Kis, A. *ACS Nano* **2011**, *5*, 9703−9709.

DOI: 10.1021/acs.nanolett.5b03481
Nano Lett. 2016, 16, 188−193

(19) Wagner, P.; Ivanovskaya, V. V.; Rayson, M. J.; Briddon, P. R.; Ewels, C. P. *J. Phys.: Condens. Matter* **2013**, *25*, 155302.
(20) Yamamoto, M.; et al. *ACS Nano* **2014**, *8*, 3895−3903.
(21) Cooper, R.; Lee, C.; Marianetti, C.; Wei, X.; Hone, J.; Kysar, J. *Phys. Rev. B: Condens. Matter Mater. Phys.* **2013**, *87*, 035423.
(22) Duerloo, K. A.; Li, Y.; Reed, E. J. *Nat. Commun.* **2014**, *5*, 4214.
(23) Zhao, J.; Kou, L.; Jiang, J. W.; Rabczuk, T. *Nanotechnology* **2014**, *25*, 295701.
(24) He, K.; Poole, C.; Mak, K. F.; Shan, J. *Nano Lett.* **2013**, *13*, 2931−2936.
(25) Kim, Y.; et al. *Nano Lett.* **2013**, *13*, 4068−4074.
(26) Lu, H.; Bark, C. W.; Esque de los Ojos, D.; Alcala, J.; Eom, C. B.; Catalan, G.; Gruverman, A. *Science* **2012**, *336*, 59−61.
(27) Jerominek, H.; Picard, F.; Vincent, D. *Opt. Eng.* **1993**, *32*, 2092−2099.

DOI: 10.1021/acs.nanolett.5b03481
Nano Lett. 2016, 16, 188−193